THE INFLUENCE OF DC STRAY CURRENT ON STEEL FIBER REINFORCED CONCRETE CORROSION

Longbin LIN [1,*], Ruiqi YANG [2]

Based on the service environment of subway tunnel structures, the impact of stray currents on the corrosion of steel fiber reinforced concrete (SFRC)and the effects of various factors were studied through simulated corrosion tests. Orthogonal experiments, equivalent circuit diagrams, and finite element analysis methods were applied to explore the performance of SFRC in resisting stray current corrosion. Orthogonal experiments show that conductive solutions are a significant factor affecting the strength of stray currents, and a reasonable ratio can ensure that SFRC has good anti-corrosion performance; The equivalent circuit diagram analysis shows that improving the electrical resistivity of concrete and the integrity of steel fiber passivation film can enhance the ability of SFRC to resist stray currents; Finite element analysis shows that the direction and overlap of steel fibers are the reasons for uneven corrosion of steel fibers. The findings of this research can offer valuable data support for the application of SFRC in environments with stray currents.

Keywords: steel fiber concrete, stray current, chloride ions, corrosion, corrosion inhibitor

1. Introduction

Steel fiber reinforced concrete (SFRC) as a prefabricated tunnel segment material has significant advantages, possessing high mechanical strength, good fatigue resistance, impact resistance, excellent durability, and post-cracking toughness [1,2], coupled with high fire resistance, making it an ideal material for tunnel structures. However, in the field of underground rail transit engineering, the application and promotion of SFRC have long been stagnant. The primary reason for this lies in the insufficient grasp of the corrosion resistance capacity of structural materials when steel bars are replaced by SFRC. At the same time, the market's excessive focus on material cost-effectiveness and the aversion to increased initial investment in projects have also hindered its promotion to some extent. Therefore, in-depth exploration of the corrosion resistance of SFRC in stray current environments is of great engineering significance.

In recent years, numerous scholars both domestically and internationally have conducted extensive research on the impact of stray currents on SFRC

[1] School of Civil Engineering, Xiamen University, Tan Kah Kee College, Zhangzhou, China, *Corresponding author, e-mail: llb@xujc.com
[2] School of Architecture and Civil Engineering, Xiamen University, Xiamen, China.

corrosion and have achieved a series of results. Aoki et al. [2] and Raczkiewicz et al. [3] found that the addition of steel fibers can enhance the corrosion resistance of reinforced concrete and inhibit the corrosion of steel bars. The research results of Feng et al. [4] and Wilkinson and Tang [5] consistently show that the coupling effect of stray currents and chloride ions will significantly aggravate the corrosion degree of steel fibers. Stray currents not only expedite the ingress of chloride ions but also facilitate the corrosion of steel fibers. When the chloride ion concentration exceeds a certain threshold, this exacerbating effect becomes more obvious. Tang [6] also found that in a chloride ion-free environment, SFRC exhibits high resistance to stray current corrosion. The research by Mauro et al. [7] revealed the influence of the aspect ratio, content, and corrosion degree of steel fibers on the bending performance of SFRC, among which the impact of the corrosion degree is particularly significant and cannot be ignored. Liu et al. [8] found that the mechanical properties of SFRC will gradually weaken under the action of stray currents, while the addition of fly ash and slag can enhance the stray current corrosion resistance of SFRC. Solgaard et al. [9] studied the influence of steel fiber volume fraction and concrete humidity on the resistivity of SFRC, and the results showed that humidity has a significant impact on the resistivity of SFRC. Chen et al. [10] found that the larger the crack width of ultra-high-performance concrete (UHPC), the faster the chloride ion penetration rate and the more severe the steel fiber corrosion, while stray currents significantly accelerate the transmission speed of chloride ions in the cracks. Chen et al. [11] designed a set of corrosion simulation systems to study the influence of stray currents and high water pressure on the penetration of chloride ions in UHPC. The research findings indicated that stray current is the primary factor influencing the transport of chloride ions, and its coupling effect with high water pressure further accelerates chloride ion transport. Pyo et al. [12] showed that ultra-high-performance concrete (UHPC) mixed with steel fibers has good resistance to chloride ion penetration. Specimens with a thickness greater than 25mm showed no significant decrease in compressive strength and flexural performance after soaking in sodium chloride solution for 365 days. Gao [13] et al. found that the durability of UHPC is severely insufficient in a stray current environment, but the incorporation of phosphorus slag powder and fly ash helps to enhance its corrosion resistance. Guo et al. [14,15] studied the corrosion law of steel fibers in cementitious materials under the coupling effect of stray currents and chloride ions, as well as the relationship between the resistivity of steel fiber concrete and the length of the material specimen. Munot [16] found that coating anti-corrosion coatings on the surface of low-carbon steel can significantly improve its corrosion resistance, but this performance will fail in high-concentration chloride ion environments. While the aforementioned research has yielded certain outcomes, there are still many problems to be solved regarding the

characteristics of SFRC resisting stray current corrosion, especially in terms of corrosion mechanisms.

Based on this, this paper carefully designed a set of stray current corrosion simulation devices to deeply study the time-varying law of corrosion current of SFRC specimens under the action of stray currents, analyzed the key factors affecting the maximum corrosion current, and discussed the mechanism of steel fiber rusting. By adopting the orthogonal experimental method, the action laws of key factors such as conductive solution, concrete resistivity, and steel fiber passivation film integrity were successfully discovered, providing quantitative indicators and theoretical basis for optimizing the mix ratio of SFRC and improving its corrosion resistance. Using corrosion equivalent circuits and electric field distribution simulation techniques, the influence mechanism of steel fiber direction and lap joint on rust distribution was revealed, and the corrosion behavior of SFRC in a stray current environment was explained from a microscopic level. This research aims to reveal the corrosion characteristics of SFRC and provide scientific and accurate guidance for engineering practice.

2. Orthogonal Experimental Design

The objective of the experiment is to investigate the corrosion impact of various factors on SFRC and analyze the optimal combination for SFRC to resist stray current corrosion. The experimental scheme uses the maximum corrosion current value as the indicator and considers steel fiber volume fraction (A), fly ash blending ratio (B), rust inhibitor blending ratio (C), and conductive solution (D) as influencing factors. Each influencing factor is set at 3 levels, as shown in Table 1. The conductive solutions in the table are saturated $Ca(OH)_2$ solution, 3% mass fraction NaCl solution, and tap water.

Table 1

Level value information table

Level	Factor			
	A/%	B/%	C/%	D
1	0.5	0	0	$Ca(OH)_2$
2	1.0	15	2	NaCl-3%
3	1.5	30	4	Water

2.1 Specimen Design

The designed strength of SFRC is C40, and the water-binder ratio is 0.41. The steel fiber used in the specimens is a sheared type with a length of 30mm, an equivalent diameter of 0.5mm, an aspect ratio of 60.2, and a tensile strength of 620MPa. The chemical composition is detailed in Table 2. The cement is Conch brand P.O 42.5 cement, the fly ash is Class F Grade II, the sand is river sand, the crushed stone is granite crushed stone (particle size 10mm~20mm), the water

reducing agent is pohnt-ys type air-entraining water reducing agent produced by Kezhijie New Material Group, and the rust inhibitor is KJ-R steel bar rust inhibitor produced by Xiamen Kaijing Industry Co., Ltd.

According to the orthogonal experimental method, a total of 9 groups of concrete with different mix proportions were designed, as shown in Table 3. The specimens were subjected to standard curing. After 28 days of curing, they were moved to an indoor environment for natural air drying. The age of the specimens was 300 days during the corrosion test.

Table 2

Chemical composition of steel fiber %

C	Si	Mn	P	S	Alt	N
0.05	0.01	0.23	0.01	0.01	0.04	0.004

Table 3

Concrete mix proportion

Number	Steel fiber/ kg	Water/ kg	Cement/ kg	Fly ash/ kg	Sand/ kg	1~2Stone/ kg	Water reducer/ kg	Rust inhibitor/ kg	Slump/cm
M 1	39.25	166	405	0	717	1075	7.29	16.2	18
M 2	78.50	168	410	0	750	1035	8.20	0.0	9
M 3	117.75	170	415	0	781	995	9.13	8.3	12.5
M 4	39.25	166	344	61	717	1075	8.10	8.1	10
M 5	78.50	168	349	61	750	1035	8.61	16.4	17
M 6	117.75	170	353	62	781	995	9.96	0.0	16
M 7	39.25	166	284	122	717	1075	8.12	0.0	13
M 8	78.50	168	287	123	750	1035	8.61	8.2	19
M 9	117.75	170	291	125	781	995	10.83	16.6	17

Note: The specimen size is 100mm×100mm×100mm.

2.2 Experimental Setup

During the operation of subway trains, a portion of the current returning through the running rails leaks due to factors such as rail resistance and potential difference to the ground, which is known as stray current. Stray current may flow into structural materials, causing corrosion, and then flow out of the materials back to the running rails. This study utilizes the experimental configuration illustrated in Fig. 1 to replicate the ingress of stray current into structural materials and conduct corrosion tests. In this setup, as shown in Fig. 1, the graphite plate is interfaced with the positive terminal of the DC power supply, the titanium mesh is connected to the negative terminal, and a paperless recorder is employed to log the current measurements. The working principle is as follows: current is output from the positive pole of the power supply, transmitted to the graphite plate, reaches the cathode surface of the specimen through the conductive solution in the anti-corrosion box, then traverses the specimen to reach the anode surface, and

ultimately returns to the negative terminal of the DC power supply via the conductive solution and the titanium mesh. The steel fibers in the SFRC are corroded when current passes through them. The internal and external joints of the anti-corrosion box and the specimen are sealed with neutral silicone to prevent leakage of the conductive solution.

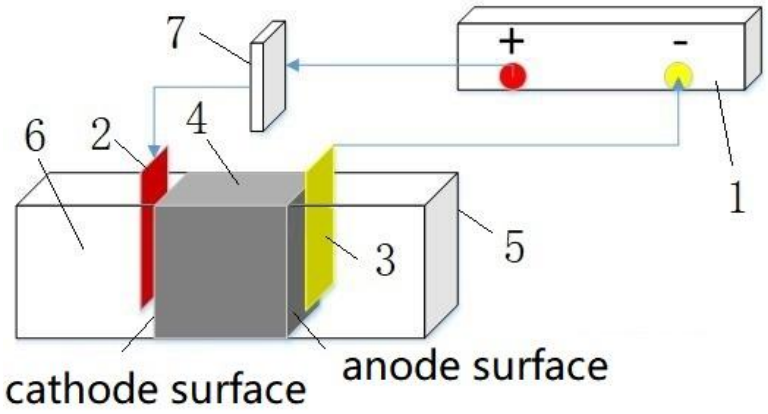

Fig. 1. Setup for corrosion test
(1. DC power supply, 2. Graphite plate, 3. Titanium mesh, 4. Steel fiber reinforced concrete specimen, 5. Anti-corrosion box, 6. Conductive solution, 7. Paperless recorder)

Referring to the research results of Guo [17], saturated $Ca(OH)_2$, tap water, and 3% mass fraction NaCl were used as conductive solutions for the tests. A total of 9 groups of corrosion tests were conducted with a test voltage of 60V and a test duration of 4320min (3 days). The conductive solution was replaced every 1440min (1 day). The experimental numbers were assigned according to the factors and levels, as shown in Table 4. The letters represent the influencing factors, and the numbers represent the levels. For example, the experimental number A3-B2-C1-D2 indicates that the steel fiber volume fraction is 1.5%, the fly ash blending ratio is 15%, the rust inhibitor blending ratio is 0%, and the conductive solution is a 3% mass fraction NaCl solution.

Table 4

Orthogonal test protocol and results

Test No.	Test Code	Concrete Mix Proportion	Maximum Current/A
1	A1-B1-C3-D2	M1	0.191
2	A2-B1-C1-D1	M2	0.118
3	A3-B1-C2-D3	M3	0.103
4	A1-B2-C2-D1	M4	0.019
5	A2-B2-C3-D3	M5	0.021
6	A3-B2-C1-D2	M6	1.000
7	A1-B3-C1-D3	M7	0.016
8	A2-B3-C2-D2	M8	0.023
9	A3-B3-C3-D1	M9	0.018

3. Experimental Results and Range Analysis

3.1 Experimental Results

There were certain differences in the current magnitude, change trend, and rusting of steel fibers among the different corrosion test groups, as shown in Figs. 2~10. In the figures, the curves represent the corrosion current values, and the three photos respectively show the rust condition on the anode surface of the specimens when the conductive solution was replaced. Mi is the mix proportion number of the specimen. The maximum current values for each test group are detailed in Table 4.

In the corrosion tests with different conductive solutions, both the corrosion current and the rust showed significant differences. Corrosion current change: In the tests with saturated $Ca(OH)_2$ and tap water as conductive solutions, the current was relatively stable or showed a gradually decreasing trend; in the tests with 3% mass fraction NaCl solution, the current fluctuated sharply or showed a gradually increasing trend. Differences in rust characteristics: In the tests with saturated $Ca(OH)_2$ conductive solution, slight pitting corrosion appeared on the anode surface of the specimens, and minor surface cracks were visible, but the corrosion developed slowly and did not extend inward, as shown in Figs. 3, 5, and 10; in the tests with tap water conductive solution, the rust on the anode surface of the specimens was slightly more severe, and the rust quantity rose in tandem with the growing steel fiber content, as depicted in Figs. 4, 6, and 8; in the tests with 3% mass fraction NaCl solution, the rust was the most severe, and the difference in the amount of rust among different groups was significant, as shown in Figs. 2, 7, and 9.

The rusting of specimen A3-B2-C1-D2 was the most severe, with the anode surface completely covered by rust, as shown in Fig. 7. Cracks formed on the anode surface, side surface, and cathode surface of the specimen, interconnected and extending into the interior of the specimen, as illustrated in Fig. 11. The cracks on the cathode surface had the largest width but the least amount of rust products, followed by the side surface, and the cracks on the anode surface had the smallest width but the most rust products. The rusting of steel fibers inside the specimen varied greatly and could be divided into three situations: intact, corrosion at one end, and comprehensive severe corrosion, as shown in Fig. 12.

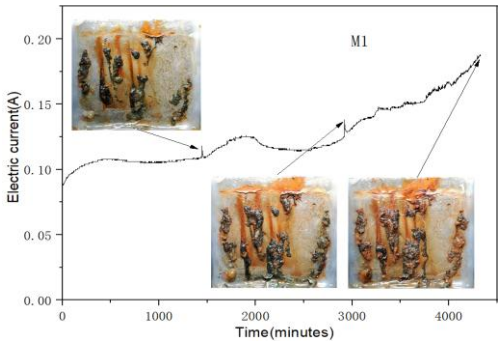

Fig.2. A1-B1-C3-D2current curve

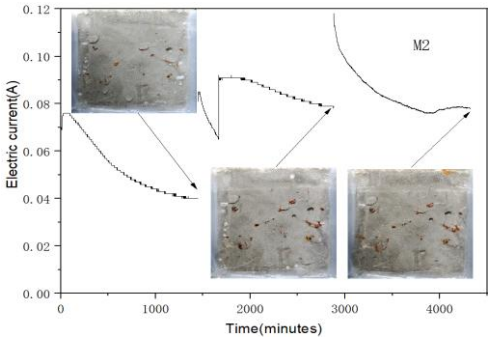

Fig.3. A2-B1-C1- D1 current curve

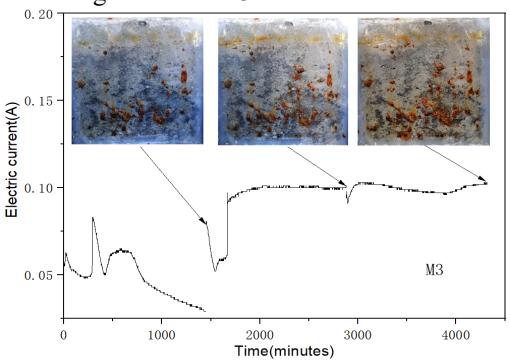

Fig.4. A3-B1-C2- D3current curve

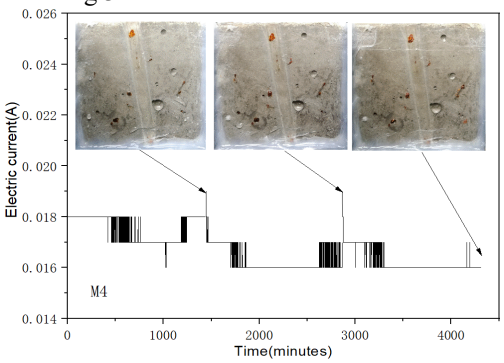

Fig.5. A1-B2-C2-D1 current curve

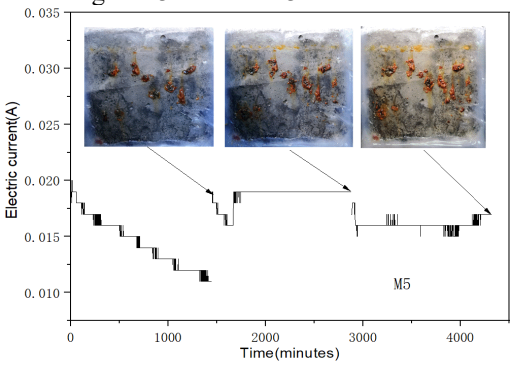

Fig.6. A2-B2-C3-D3current curve

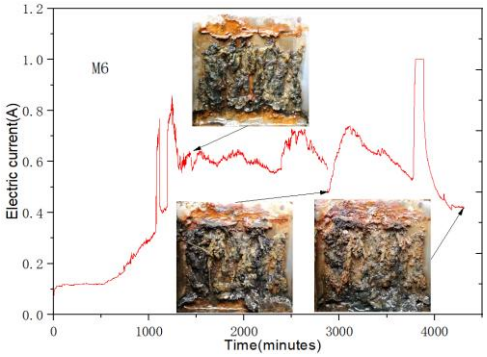

Fig.7. A3-B2-C1-D2 current curve

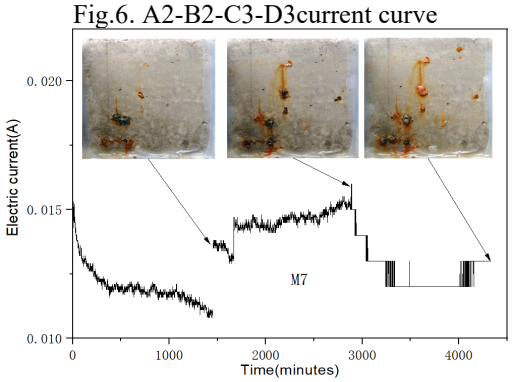

Fig.8. A1-B3-C1-D3current curve

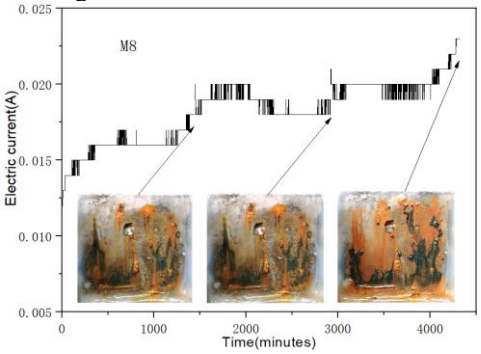

Fig.9. A2-B3-C2-D2 current curve

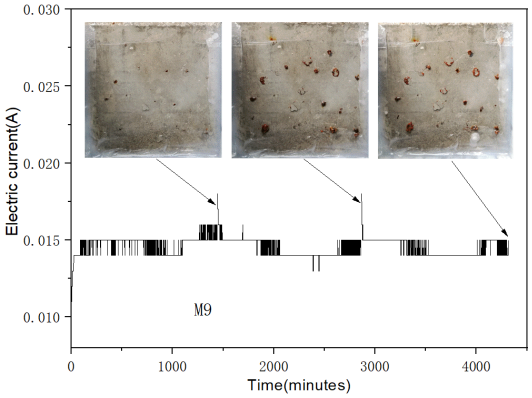

Fig.10. A3-B3-C3-D1current curve

(a) anode surface (b) lateral side (c) cathode surface

Fig.11. A3-B2-C1-D2 photos of specimen cracks

(a) no corrosion (b) end corrosion (c) total corrosion

Fig. 12. Photos of rusted steel fibers in A3-B2-C1-D2

3.2 Range Analysis

To quantify the individual impact of the four factors (A–D) on the stray-current corrosion sensitivity of SFRC, a range analysis was applied to the orthogonal test data, with the maximum current Imax as the response variable (lower Imax indicates better corrosion resistance). The results in Table 5 show the significance sequence D > C > B > A. Factor D, the conductive solution, exhibits the largest range, indicating that chloride-bearing environments markedly amplify the stray current. Factors C (inhibitor dosage) and B (fly-ash content) display

comparable ranges; both reduce the corrosion current by increasing matrix resistivity or preserving the passivation film. Factor A (steel-fiber volume fraction) has the smallest range but remains non-negligible—excessive volume fraction creates continuous conductive paths and thus elevates the current.

Table 5

Extreme differences analysis of the orthogonal test

Indicator	Maximum Current/A			
	A	B	C	D
K_1	0.226	0.412	1.134	0.155
K_2	0.162	1.04	0.145	1.214
K_3	1.121	0.057	0.230	0.140
k_1	0.075	0.137	0.378	0.052
k_2	0.054	0.347	0.048	0.405
k_3	0.374	0.019	0.077	0.047
Range R	0.320	0.328	0.330	0.358

In Table 5, K_i denotes the sum of Imax values for all runs that include level i of a given factor; the mean value k_i is calculated as K_i / t, with t = 3 being the number of occurrences of each level in the orthogonal array; the range R = max(k_i) – min(k_i) indicates the sensitivity of Imax to changes in factor level, with larger R signifying greater influence.

The trend of the maximum current value with the four factors is depicted in Fig. 13. From Fig. 13, it is evident that the maximum current value first decreases and then increases with the increase of steel fiber volume fraction; it initially rises and subsequently falls as the fly ash content increases; it first decreases and then increases with the increase of rust inhibitor content; and it first increases and then decreases with the change of conductive solution, with D3 being the optimal conductive solution. Selecting the level corresponding to the minimum K_i for each factor yields the optimal stray-current-resistant formulation A2-B3-C2-D3, and tap water as the conductive solution.

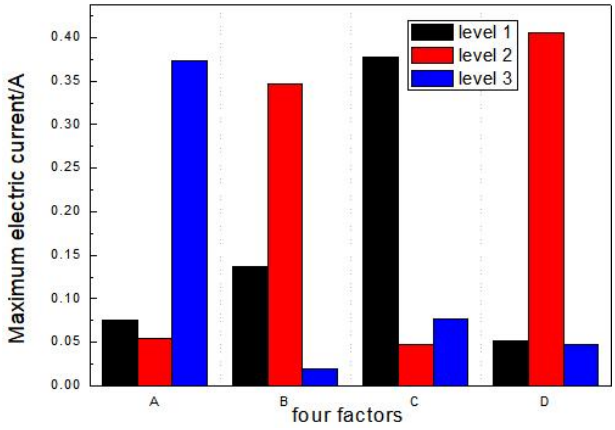

Fig. 13. The max electric current varied with four factors

4. Mechanism Analysis

4.1 Equivalent Circuit Diagram Analysis

The experiment can be described by the equivalent circuit diagram in Fig. 14. I is the experimental current collected by the recorder, R_{d1} is the resistance of the conductive solution between the graphite plate and the anode surface of the specimen, R_{d2} is the resistance of the conductive solution between the titanium mesh and the cathode surface of the specimen, R_{ij} represents the combined resistivity of the passivation film and concrete between two adjacent steel fibers through which current flows, and R_{n+1} is the resistivity of the concrete in the current path that does not flow through the steel fibers. In the experiment, the main factors affecting the intensity of the corrosion current are R_{d1}, R_{d2}, R_{ij}, and R_{n+1}. The resistance value of the SFRC specimen is represented by the following equation:
(1)

$$R = \frac{1}{\frac{1}{\sum R_{1i}} + \frac{1}{\sum R_{2j}} + \cdots + \frac{1}{\sum R_{nk}} + \frac{1}{R_{n+1}}} \tag{1}$$

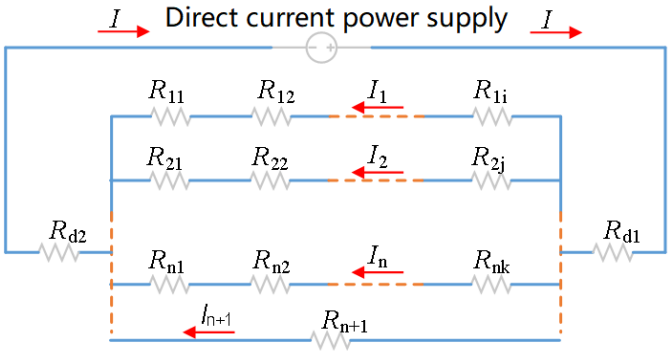

Fig. 14. Experimental equivalent circuit diagram of stray current corrosion

Current enters the material from the anode surface and is randomly divided into n+1 current paths. The current is affected by the resistance of each path, $\sum_{k=1}^{k} R_{ik}$ and R_{n+1}, where R_{ik} is the sum of the resistivity of the passivation film and concrete between the k segments of steel fibers in the i-th current path. Owing to the incorporation of steel fibers, the propagation distance of current in the concrete

matrix is reduced, i.e., $\sum_{k=1}^{k} R_{ik}$ becomes smaller. According to Equation (1), the resistance value R of the concrete will become smaller, which is consistent with the research results in the literature [9]. Due to the differences in the direction distribution and possible lap joints of steel fibers, there are differences in the resistivity of each path, leading to variations in the current intensity passing through the steel fibers.which is the reason for the different degrees of rusting of the steel fibers. It can be seen from Equation (1) that R_{ij} and R_{n+1} are important factors affecting the corrosion current. Increasing the resistivity of the concrete and maintaining the integrity of the passivation film can increase the resistivity of SFRC and enhance its ability to resist stray current corrosion.

4.2 Steel Fiber Corrosion Analysis

The high alkalinity of concrete provides a good protective environment for preventing steel fiber corrosion. About 1/5 of the hydration reaction products in cement are calcium hydroxide, and the pH value can reach 13. This alkaline environment facilitates the development of a passivation film on the metal surface, which can well protect the steel fibers from corrosion. Stray current, however, can damage the passivation film and has a negative effect on its formation [18-19]. In the tests numbered 4, 5, 7, 8, and 9, the maximum corrosion current intensity was small, and the adverse impact of stray current was less pronounced than the beneficial effect of the alkaline environment, so the steel fibers were well protected. The test results align with the characterization of the physical properties and durability of SFRC as described by the American Concrete Institute (ACI). ACI Report 544 states that "because the fibers are short and discontinuous, with little overlap between them, stray currents generated by electromotive forces in different areas of the concrete do not have continuous conductive paths" [20]. In practical engineering, enhancing the compactness and carbonation resistance of concrete to sustain a high pH value serves as an effective strategy to bolster the resistance of SFRC against stray current corrosion.

The synergistic action of chloride ions and stray current exhibits strong corrosive properties, and the corrosion resistance of SFRC is greatly challenged. In the tests numbered 1, 6, and 9, the reasons for the increasing trend of corrosion current are: 1) Stray current increases the permeability of concrete [21], the diffusion coefficient of chloride ions [5], and the conductivity of the concrete pore solution; 2) The conductive solution penetrates into the cracks formed by rust expansion, enhancing the conductivity of the material; 3) Ion migration causes an increase in the pore volume of the concrete [21], the microstructure is damaged [22], and the internal structure becomes loose, leading to a decrease in resistivity; 4) Damage to the passivation film and a decrease in its resistivity [23] lead to a

decrease in the resistivity of SFRC. The reasons for steel fiber corrosion are: 1) Under the influence of stray current, the detrimental impact of chloride ions on the metal passivation film is markedly intensified. 2) The formation of cracks and the impairment of the microstructure facilitate the ingress of chloride ions.3) The continuous destruction of the alkaline environment hinders the formation of the passivation film, indirectly reducing the corrosion resistance; 4) Steel fibers undergo severe corrosion under the combined action of multiple unfavorable factors.

Appropriate mix proportion design can bolster the resistance of SFRC to the synergistic corrosion effects of stray current and chloride ions. As shown in Table 4, the maximum current intensity in Test No. 8 with NaCl as the conductive solution is only 0.023A, which is lower than the maximum current intensity of 0.118A in Test No. 2 and 0.103A in Test No. 3 with other conductive solutions. The SFRC with mix proportion M8 exhibits excellent resistance to the coupled erosion of stray current and chloride ions, The SFRC specimen with the M8 mix proportion demonstrates outstanding resistance to the combined erosion effects of stray current and chloride ions. mainly benefiting from the 30% blending ratio of fly ash and the 2% blending ratio of rust inhibitor. Fly ash can reduce the porosity of concrete, the permeability to water and gas, and increase the resistivity of concrete [24]. Research in [25] shows that when the fly ash blending ratio is within 30%, the water and gas permeability coefficients of concrete decrease significantly with the increase of the blending ratio, and [26] also mentions that concrete has a better pore structure when the fly ash blending ratio is 30%. Rust inhibitors can improve the resistance of concrete to chloride ion intrusion, alleviate the damaging effect of chloride ions on the metal passivation film [27], and inhibit the destructive effect of chloride ions on steel corrosion [28]. The experiment indicates that rational mix proportion design can ensure the structural safety of SFRC under the influence of stray current.

4.3 Finite Element Analysis

ANSYS application software can be used for simulation of engineering structures, electromagnetics, heat transfer, fluid dynamics, and coupled or multiphysics fields. In this paper, the "PLANE121" element of this software was selected to perform a two-dimensional simulation of the stray current corrosion simulation experiment. The concrete specimen model had dimensions of 0.1m × 0.1m, the relative dielectric constant of the material was set to 15, and the resistivity was 50kΩ•m. The voltage boundary conditions on the left and right sides of the model were set to 10V and 0V, respectively, simulating the potential difference across the specimen. Six steel fibers with different orientations were arranged within the model, with dimensions of 0.03m × 0.0005m. The dielectric constant of the steel fiber material was set to 10^7, and the resistivity was 10^{-7} kΩ•m. By

calculating the distribution of the electric field strength inside the specimen, the relationship between the electric field strength and the orientation and overlap of the steel fibers was analyzed.

The electric field intensity in the concrete surrounding the ends of the steel fibers is influenced by the fiber orientation. From Fig. 15(a), it can be seen that the longer the projection distance of the steel fiber in the direction of voltage gradient change, the greater the electric field strength in the concrete at the ends of the steel fiber, i.e., the more current flows through the steel fiber; when the steel fiber is perpendicular to the direction of voltage gradient change, the current intensity near the steel fiber is smaller, and less stray current flows through the steel fiber. The simulation results explain the reason for the large differences in steel fiber corrosion.

The overlap of steel fibers affects the electric field strength in the concrete at the ends of the fibers. The longer the projection length of the overlapped steel fibers in the direction of voltage gradient change, the greater the electric field strength at both ends of the steel fibers, as shown in Fig. 15(b). The current intensity flowing through the overlapping steel fiber path is associated with the fiber's projection length in the direction of the voltage gradient change. A longer projection length corresponds to a larger electric field strength at the ends of the fiber and a larger current flowing through the steel fiber. The simulation outcomes align with the analysis derived from the equivalent circuit diagram. Therefore, improving the uniformity of steel fiber distribution within the concrete and reducing steel fiber overlap and clustering helps to resist current flow.

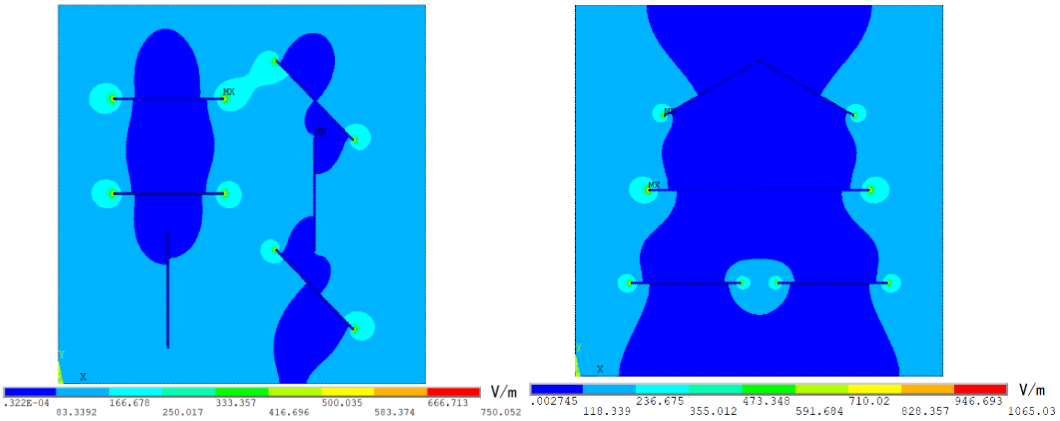

(a) Steel fiber no lap situation (b) Steel fiber lap situation

Fig. 15. Plots of electric field strength in different cases

5. Conclusions

In this study, the corrosion performance of steel fiber reinforced concrete (SFRC) in a stray current environment was investigated in depth using orthogonal

experiments, equivalent circuit diagrams, and finite element analysis. Some beneficial conclusions were obtained:

Conductive solution is a significant factor affecting the maximum stray current value. Stray current not only promotes the electrochemical corrosion of metal but also enhances the ability of chloride ions to invade concrete and damage the passivation film on the surface of steel fibers. The synergistic interaction of these two factors is the primary cause of the severe corrosion of steel fibers in SFRC.

The resistivity of concrete and the passivation film of steel fibers are important internal factors affecting the resistance of SFRC to stray current corrosion, while chloride ion intrusion is an important external factor. Through reasonable mix proportioning, the compactness of concrete can be improved, and the integrity of the steel fiber passivation film can be protected, which is an effective measure to enhance the durability of SFRC.

The extent of steel fiber corrosion is influenced by the fiber orientation and overlap. The extent of steel fiber corrosion is inversely proportional to the angle between the longitudinal direction of the steel fiber and the direction of the potential gradient; the smaller the angle, the more pronounced the corrosion. When steel fibers overlap, the electric field strength at the ends of the steel fibers is greater than that without overlap, resulting in a larger corrosion current and more severe corrosion.

The results of Test No. 8 show that even in the harsh environment of stray current and chloride ion co-action, a proper mix proportion can still ensure that SFRC has good corrosion resistance. This finding offers robust experimental support for the application of SFRC in subway projects.

This research reveals the influence law of conductive solution, concrete resistivity, and steel fiber passivation film integrity on the corrosion performance of SFRC through interdisciplinary research methods, providing a new perspective for the corrosion theory of steel fiber concrete, which has theoretical significance.

Acknowledgement

The second batch of science and technology plan projects in 2023 for the housing and urban and rural construction industry in Fujian Province, the development and application of the health monitoring system for water supply and drainage pipelines in soft soil foundation based on the Internet of Things (No. 2023-K-75)

REFERENCES

[1] Angelo Caratelli, Alberto Meda, Zila Rinaldi, et al. Optimization of GFRP reinforcement in precast segments for metro tunnel lining. Composite Structures, 2017, 181: 336-346.

[2] Hiroaki Aoki, Zhao Wang, Mingqian Ren, et al. Experimental investigation of the electro-chemical characteristics of SFRCs under the effect of chloride ion intrusion. Construction and Building Materials, 2024, 457: 139345.
[3] Wioletta Raczkiewicz, Magdalena Bacharz, Kamil Bacharz, et al. Reinforcement Corrosion Testing in Concrete and Fiber Reinforced Concrete Specimens Exposed to Aggressive External Factors, 2023: 1-19.
[4] Weipeng Feng, Anel Tarakbay, Shazim Ali Memon, et al. Methods of accelerating chloride-induced corrosion in steel-reinforced concrete: A comparative review. Construction and Building Materials, 2021, 289: 123165.
[5] Stephen Wilkinson, Kangkang Tang. Corrosion Resistance of Steel Fiber Reinforced Tunnels Subject to Stray Current: Springer Nature Singapore, 2024: 505-511.
[6] Kangkang Tang. Stray alternating current (AC) induced corrosion of steel fiber reinforced concrete. Corrosion Science, 2019, 152: 153-171.
[7] Mauro Fernandes, Rui Neves. Assessment of Fiber Corrosion Influence in the Flexural Performance of Steel Fiber-Reinforced Concrete. Applied Sciences, 2024: 1-13.
[8] Haotian Liu, Lin Yang, Kailong Kang, et al. Mechanical properties and corrosion mechanism of steel fiber reinforced concrete (SFRC) subjected to stray current. Journal of Building Engineering, 2024, 96: 110519.
[9] Anders Ole Stubbe Solgaard, Mette Geiker, Carola Edvardsen, et al. Observations on the electrical resistivity of steel fiber reinforced concrete. Materials and Structures, 2014, 47: 335-350.
[10] Ming-Yue Chen, Ren-Peng Chen, Yong-Qing Chen, et al. Stray current induced chloride ion transport and corrosion characteristics of cracked ultra-high performance concrete. Construction and Building Materials, 2023, 398: 132536.
[11] Mingyue Chen, Xin Kang, Yongqing Chen, et al. Unveiling the synergistic effects of stray current and high hydraulic pressure on chloride transport in ultra-high-performance concrete. Cement and Concrete Composites, 2025, 157: 105957.
[12] Sukhoon Pyo, Taehoon Koh, Million Tafesse, et al. Chloride-induced corrosion of steel fiber near the surface of ultra-high performance concrete and its effect on flexural behavior with various thickness. Construction and Building Materials, 2019, 224: 206-213.
[13] Gao Dejun, Huang Yulong, Wang Qing, et al. Research on the Deterioration Characteristics of UHPC in Stray Current Environment. Bulletin of the Chinese Ceramic Society, 2023, 42(06): 2007-2014.
[14] Guo Liping, Yang Bo, Chen Bo, et al. The corrosion resistance of fiber-reinforced mortar under the coupling effect of stray current and chloride ions. Journal of Water Resources and Architectural Engineering, 2016, 14(02): 11-17.
[15] Guo Liping, Ding Cong, Yang Bo, et al. Analysis of resistivity of steel fiber Reinforced Concrete and Reinforced concrete. Journal of Hebei University of Technology, 2014, (06): 26-29.
[16] Hema Munot, Pravin Deshpande, Chetankumar Modhera. Effects of chloride ions on the corrosion resistance of conducting polypyrrole coated steel in simulated concrete pore solution. UPB Scientific Bulletin, Series B: Chemistry and Materials Science, 2017, 79(2): 191-206.
[17] Guo Zhanrong, Huang Yipu, CAI Minggang, et al. Determination of nutrient salt content and chlorine content indicators in Groundwater of Xiamen Island. Site Investigation Science and Technology, 2004, (03): 47-50.
[18] Hu Liu,Kaibin Li,Yongqiang Li, et al. Corrosion behavior of steel fiber reinforced concrete under ambipolar stray current interference. Construction and Building Materials, 2024, 411: 134302.
[19] Wenqiang Xu, Yu Li, Hanzhang Li, et al. Corrosion mechanism and damage characteristic of

steel fiber concrete under the effect of stray current and salt solution. Construction and Building Materials, 2022, 314: 125618.
[20] Kangkang Tang. Corrosion of steel fiber reinforced concrete (SFRC) subjected to simulated stray direct (DC) interference. Materials Today Communications, 2019, 20: 100564.
[21] A. Aghajani, M. Urgen,L. Bertolini. Effects of DC Stray Current on Concrete Permeability. Journal of Materials in Civil Engineering, 2016, 28.
[22] Hongqiang Chu, Tingting Wang, Ming-Zhi Guo, et al. Effect of stray current on stability of bound chlorides in chloride and sulfate coexistence environment. Construction and Building Materials, 2019, 194: 247-256.
[23] Liu Xin, Wu Miao, Shi Jinjie. The electrochemical behavior of corrosion-resistant reinforcing bars in concrete simulation liquid. Journal of Southeast University (Natural Science Edition), 2019, 49(3): 502-506.
[24] Lin Longbin, Feng Zhengwei, Xiao Shan, et al. Research on the Resistivity of Steel Fiber Reinforced Concrete Based on Orthogonal Experiments. Fujian Architecture & Construction, 2017, 228(06): 127-129+144.
[25] Zhang Junzhi, Lyu Meng, Fang Zhaofeng, et al. Research on Water and Gas Permeability and Pore Structure of Fly Ash Concrete Based on Nuclear Magnetic Resonance. Journal of Nanchang Institute of Technology, 2018, 37(06): 63-70.
[26] Tan Yewen, Wang Shuguang, Liu Weiqing, et al. The influence of fly ash on the resistance of concrete to chloride erosion. Concrete, 2017, (07): 144-148.
[27] Fabio Bolzoni, Andrea Brenna, Marco Ormellese. Recent advances in the use of inhibitors to prevent chloride-induced corrosion in reinforced concrete. Cement and Concrete Research, 2022, 154: 106719.
[28] Shehnazdeep, Bulu Pradhan. A study on effectiveness of inorganic and organic corrosion inhibitors on rebar corrosion in concrete: A review. Materials Today: Proceedings, 2022, 65: 1360-1366.